



# Failure criteria calibration based on the triaxial compression behavior of roller compacted concrete (RCC)

Sherong Zhang · Peiyong Wei · Chao Wang · Gaohui Wang · Wenbo Lu · Kelei Cao

Received: 24 September 2019 / Accepted: 11 November 2020 / Published online: 6 January 2021  
© RILEM 2021

**Abstract** Roller compacted concrete (RCC) has been widely used in large scale constructions such as hydraulic structures and heavy-duty pavements. Understanding the failure criterion based on the compression behavior of RCC under a relatively wide range of confining pressure is essential for the better analysis and design of RCC structures subjected to potential extreme dynamic loadings. However, few experimental results of RCC under confinement are available, and, to date, no study pays close attention on the triaxial behavior of RCC under relatively high confining pressure. In this study, triaxial behavior was investigated with the aim to better understand and model the constitutive behavior of RCC material. Purposely, laboratory tests were employed on  $100 \times 200$  mm (diameter  $\times$  length) cylindrical

specimens, while the mix proportion and molding method were generally consistent with field construction. Triaxial tests were conducted under seven different confining pressure levels (0, 5, 10, 15, 20, 25 and 30 MPa). Consequently, the triaxial compression behavior of RCC was obtained and the confinement effect was illustrated. Compared with conventional concrete, the effect of confinement on the failure strength and failure strain of RCC was less pronounced. The failure criteria of RCC under a relatively wide range of confining pressure were discussed. Parameters of Mohr–Coulomb and William–Warnke failure criteria were calibrated and novel empirical formulas were proposed to illustrate the compressive meridian of RCC material.

---

S. Zhang · P. Wei · C. Wang (✉) · K. Cao  
State Key Laboratory of Hydraulic Engineering  
Simulation and Safety, Tianjin University,  
Tianjin 300072, China  
e-mail: janson126@163.com

S. Zhang  
e-mail: tjuzsr@126.com

P. Wei  
e-mail: wepy@tju.edu.cn

K. Cao  
e-mail: 3294361695@qq.com

C. Wang · G. Wang · W. Lu  
State Key Laboratory of Water Resources and  
Hydropower Engineering Science, Wuhan University,  
Wuhan 430072, China  
e-mail: wanggaohui@whu.edu.cn

W. Lu  
e-mail: wblu@whu.edu.cn

S. Zhang · P. Wei · C. Wang · K. Cao  
School of Civil Engineering, Tianjin University,  
Tianjin 300072, China



**Keywords** Roller compacted concrete (RCC) · Mechanical properties · Triaxial compression tests · Failure criterion · Stress–strain relationships

## 1 Introduction

Roller compacted concrete (RCC) is generally defined as a zero-slump concrete that has been consolidated by external vibratory rolling [1]. As a special concrete material, RCC consists of the similar material components as those of normal concrete and the difference lies in mix proportions and molding method. The RCC mixture contains less water and cement, but a relatively high-volume fly ash as supplementary cementitious material. This makes RCC mixtures much drier, and hence the molding method of conventional concrete is not applicable. Instead, the construction method of thin-layer pouring and vibratory rolling is employed, which is almost the same with Asphalt pavement construction [2, 3]. The above features bring about the following advantages: low heat of hydration, rapid construction, low construction cost and simple construction procedure [4]. Consequently, RCC has been widely used in highly-sensitive infrastructures, including heavy-duty pavements, overflow structures and hydraulic dams [2, 3, 5–8]. Potential extreme loadings (including impact of heavy-duty vehicles, earthquakes, near field detonations) are noteworthy concerns for RCC structures. In the above scenarios, RCC undergoes triaxial loadings with moderate or high confining pressures [9]. Considering the extensive use in water conservancy projects, it is vital to understand the mechanical properties of RCC under confinement.

The distinct mix proportion and layer structure of RCC may contribute to the differences in deformation and mechanical behavior [10]. Most researches have paid more attention to the basic behavior of RCC, for example: frost resistance [6], transport properties [8], interlayer treatments [2], efficacy of compaction [11–14], seepage characteristic [15], effect of leakage dissolution [16, 17], interface bonding quality [18, 19], temperature field [20–23] and mixture ratio [24–26], fly ash effect [27–29]. Some efforts have also been dedicated in the influence of layer structure, and it can be concluded that the existence of interlayer contributes to the decrease of RCC's shear and tensile

strength [2]. Recently, there is an arising concern about the safety of RCC structures under extreme dynamic loadings. Thus, studies on the dynamic mechanical properties of RCC have been conducted [10, 30–32]. According to the literature review, it can be concluded the distinct mix proportion and construction characteristic make the mechanical behavior of RCC different from conventional concrete. The interlayer in RCC probably turns to be a weak surface without proper treatment measures in the molding process. What's more, the high mass fraction of fly ash in cementitious materials results in more pores in RCC, and the porosity and size of pore decline with the extension of concrete age [29]. The increasing fly ash content also causes a reduction in compression, splitting tensile, and flexural strength values at ages up to 180 days [28]. The compressive strength of RCC has been found to be affected by both the cement hydration and compaction, which differs from conventional concrete [33]. And the difference in compressive behavior is more significant under high strain rates partially due to more pores in RCC.

Concerning triaxial mechanical properties, there have been many studies on triaxial behavior of conventional concrete and high strength concrete (HSC) under confining pressures up to 650 MPa [34–39]. Domingo et al. [37] carried out an experimental study on normal concrete under confining pressures ( $\sigma_3$ ) up to 60 MPa (about twice the uniaxial compressive strength), using  $\Phi 150 \times 300$  mm cylinders. They studied the effect of confining pressure on the brittle-ductile transition behavior. Martin et al. [36] and Xuan et al. [38] characterized the behavior of normal concrete under high confining pressures (up to 650 MPa). The effect of coarse aggregate size and cement paste volume on concrete behavior was also discussed. Xie et al. [39] studied the triaxial behavior of HSC under confining pressures ranging from 11.9 to 59.97 MPa. Correspondingly, the confinement ratios ( $\sigma_3/f'_c$ , where  $f'_c$  denotes uniaxial compressive strength) ranged from 0.1 to 0.504. The tests involved  $\Phi 55.5 \times 110$  mm cylindrical samples, with three different levels of uniaxial compressive strength. Ansari et al. [34] established an experimental program comprised of HSC at three different compressive strength levels (42, 69, and 103 MPa). The maximum of the confinement ratio was 1.0. The failure surface of HSC was determined and the effect of confining



pressure was discussed. Li et al. [35] paid close attention to the size effect of HSC specimens subjected to high confining pressure. Their results showed a slight size effect on the failure strength. However, experimental studies on RCC material under triaxial stress are relatively limited. Deng [40] performed a series of triaxial compression tests on  $150 \times 300$  mm (diameter  $\times$  length) cylinders. In their studies, the maximum of the confining pressures ( $\sigma_3$ ) and confinement ratios ( $\sigma_3/f'_c$ ) were 10 MPa and 0.62, respectively. The results showed an obvious difference in tangent modulus of elasticity and triaxial compressive strength between RCC and conventional concrete. Thus, there is a lack of experimental data on triaxial mechanical behavior of RCC under confining pressure over 10 MPa. In point of fact, the design of RCC structures and prediction of failure conditions under extreme dynamic loadings require the confined concrete behavior with high confining pressures. Furthermore, the validation of constitutive models to predict the dynamic behavior of RCC needs triaxial experimental data [31]. Particularly, parameters calibration of strength surface of dynamic constitutive models (for example, Holmquist–Johnson–Cook model, Karagozian & Case Concrete model) for RCC requires triaxial test data under a wide range of confining pressures. Considering the differences between RCC and conventional concrete in mechanical properties, it's urgent to conduct experiments to reveal the triaxial mechanical behavior of RCC under moderate or even high confining pressure.

In this paper, a parametric experimental study consisting of a series of triaxial tests with confining pressure up to 30 MPa was undertaken. The primary differences between this study and the available literature have been shown as follows:

- (1) An experimental program was established to simulate the field construction method of RCC, including paving and compacting using vibratory rollers;
- (2) A wide range of confining pressures ( $\sigma_3$ ) from 0 to 30 MPa ( $\sigma_3/f'_c \approx 2.0$ ) was employed in this paper, to complement the triaxial test data of RCC under moderate and high confining pressures;
- (3) The relationship between the peak axial strain ( $\varepsilon_{1p}$ ) of RCC and confining pressure is proposed in this study;

- (4) The volumetric strain history of RCC under triaxial compression is given, and the effect of confining pressures on volumetric strain history is studied;
- (5) Parameters of Mohr–Coulomb failure criterion and William–Warnke failure criterion of RCC material are calibrated.

## 2 Experimental program

Given the impact of mix proportion and layer structure on the mechanical properties of RCC, an experimental program was established to simulate the vibration compaction method in field construction.

## 3 Materials

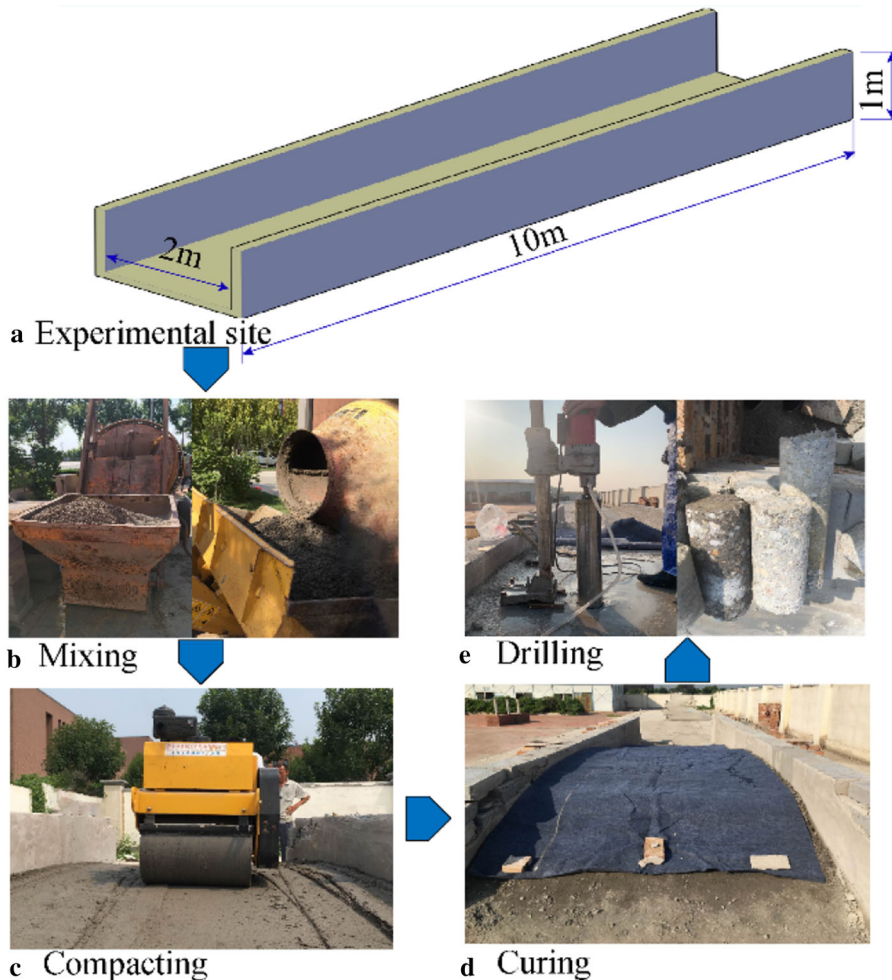
P.MH42.5 (moderate heat Portland cement) was used as the cementitious material. Class II fly ash was used as supplementary cementitious materials. The water-binder ratio was 0.50, and the fly ash content in cementitious materials was about 60% by mass. Moreover, chemical admixtures were employed to provide fluidity and workability, including the JM-II retarding superplasticizer and HLAE air-entraining agent. The characteristic properties of the above materials are within the corresponding allowed ranges in Chinese regulations [41–43]. The coarse aggregate used was crushed limestone with a maximum particle size of 20 mm. The fine aggregate was natural river sand with fitness modulus of 2.5, and the sand ratio was 31%. Based on the mix proportion in Huangdeng project, the coarse aggregate gradation was determined by method of similar grading preliminarily [44]. According to the performance of mixture and bearing capacity of concrete specimens, the mix proportion in present study were determined [30, 45], as shown in Table 1.

## 4 Specimen production

In this study,  $\Phi 100$  mm  $\times$  200 mm cylindrical specimens were employed in uniaxial and triaxial compression tests. To acquire RCC cylindrical

**Table 1** Mixing proportions of the fresh concrete mixes

Mixture	Cement (kg/m <sup>3</sup> )	Sand (kg/m <sup>3</sup> )	Fly ash (kg/m <sup>3</sup> )	Water reduce agent (kg/m <sup>3</sup> )	Air entraining agent (kg/m <sup>3</sup> )	Gravel (kg/m <sup>3</sup> )		
						4.75–9.5 mm	9.5–16 mm	16–19 mm
RCC	94	748	151	1.47	0.315	522.4	391.8	391.8

**Fig. 1** The preparation process of RCC

specimens, a specific specimen production process was designed. The details are described as follows:

1. An experimental site with dimensions of 10.0 m × 2.0 m × 1.0 m was built for the placement of eight RCC lifts, as shown in Fig. 1a. Mentioned that the average thickness of the RCC lift was 0.1 m.
2. Concerning the mixing sequence, the dry materials (coarse aggregates, fine aggregates, cement, fly ash) were mixed for 1 min, then the water was added and mixed for a further 2 min, giving a homogenous mixing by using a concrete pan mixer. The VC value of the mixture was measured to be 4.1 s, according to the test code for hydraulic concrete [42].

3. A vibratory roller (model DC25-C) with a frequency range of 0 Hz–70 Hz was used to compact the RCC mixture. The fresh RCC mixture was spread and paved to achieve the designed lift thickness. Rolling technique of “two static rolling + eight vibration rolling + two static rolling” was adopted, where the objective of static rolling was to form a smooth surface. The vibration frequency was approximately 50 Hz during vibration rolling. Noted that the average roller velocity was controlled to 0.24 m/s. After the finish of the compaction of the lower lift, an upper lift was paved and compacted.
4. When the compaction of all eight lifts was accomplished, a cushion was bedded to cure with sprinkling water for 90 days. A series of cores (100 mm in diameter) were drilled with a water-cooled diamond drill. Then the cores, used for compression tests, were cut to lengths of 200 mm and ground in both ends to ensure plane loading surfaces.

The preparation process mentioned above is illustrated in Fig. 1, more related details can be found in previous studies [10, 30, 32, 45]. It should be noted

that drilling and grinding have a limited effect on experimental results because the diameter of RCC specimens is large enough.

## 5 Apparatus and testing methods

The uniaxial and triaxial compression tests were performed at State Key Laboratory of Hydraulic Engineering Simulation and Safety, Tianjin University. The triaxial system is shown in Fig. 2. The confining pressure of this cell could be up to 100 MPa, while the loading mode can be switched between displacement control and load control. The confining pressure  $\sigma_3$  can be directly measured by a pressure transducer inside the intensifier. While axial load  $F_d$  is applied by an axial actuator and measured by an in-vessel load cell. The actual axial stress  $\sigma_1$  can be expressed as Eq. (1):

$$\sigma_1 = F_d/A_s + \sigma_3 \quad (1)$$

where  $A_s$  is the cross-sectional area of the specimen.

In this study, axial extensometer and circumferential extensometer were employed to measure axial

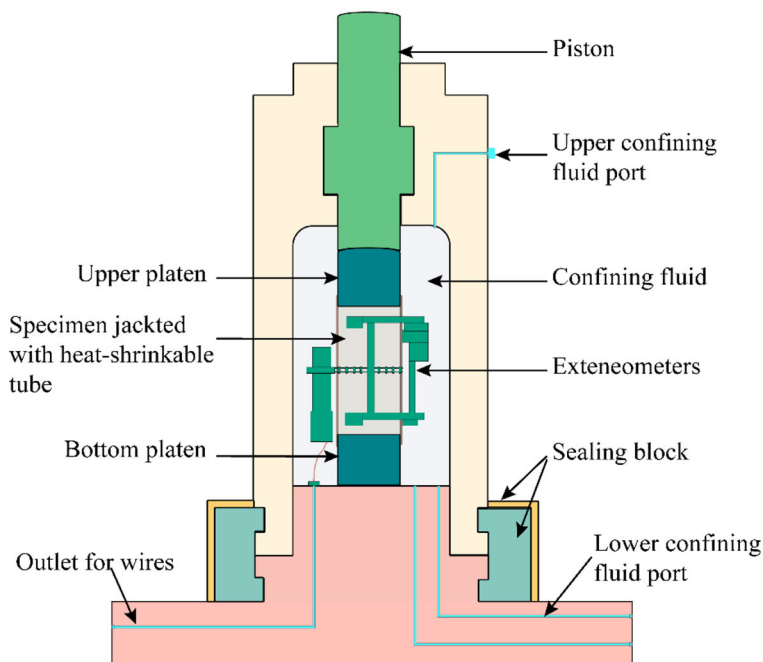


**Fig. 2** The present triaxial system



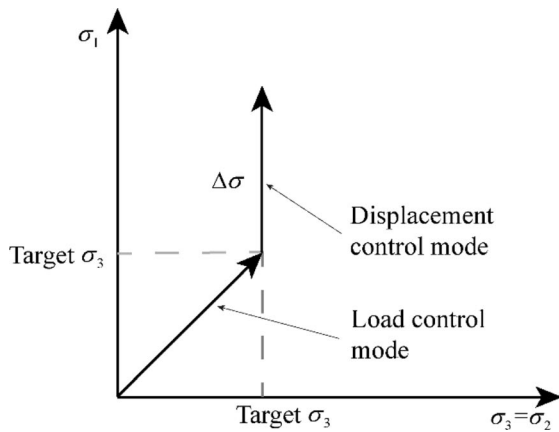


**Fig. 3** Loading path for triaxial tests

displacement and circumferential deformation, respectively. In this way, the total circumferential deformation along the whole perimeter of the cylinder can be obtained, which was utilized to derive the average lateral strain  $\varepsilon_3$ .

Under uniaxial compression, a displacement control mode was used to obtain the stress–strain curve, with a rate of 0.002 mm/s. As for triaxial compression tests, the load path is given in Fig. 3. As shown, the confining pressure was firstly applied to the target value in load control mode and then kept constant. After the target  $\sigma_3$  was obtained, the control mode was switched to displacement control and deviatoric was applied all the way up to the fracture of the RCC specimens, with a rate of 0.002 mm/s.

The penetration of confining fluid into the concrete has a significant influence on results of triaxial tests [46–48]. In this study, concrete specimens were jacketed with heat shrinkable tube (1.5 mm thick) to prevent penetration of oil. Since end-friction effect on concrete stress–strain behavior under compression is nonnegligible [49–52], a combination of two 0.125 mm-thick Teflon sheets on top of one layer of 0.015 mm thick aluminum foil was used to minimize this effect.

A total of seven levels of confining pressure ( $\sigma_3$ ) were employed to cover the response under both moderate and high confinement: 0, 5, 10, 15, 20, 25, and 30 MPa, corresponding to confinement ratios of about 0.00, 0.34, 0.67, 1.01, 1.34, 1.68, and 2.01, respectively. Mention that at least three reasonable test results were obtained at each confinement level.

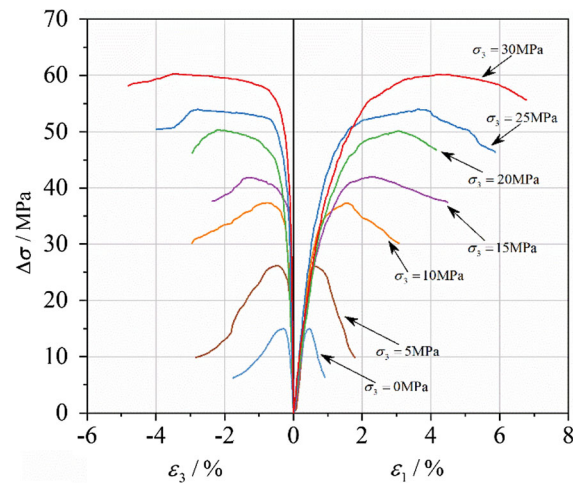
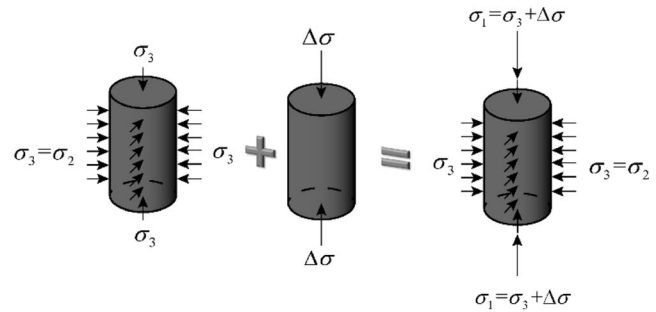


**Fig. 4** Axial deviatoric stress versus strain curves for RCC samples under confining pressures

## 6 Result and discussion

In this section, the compressive strain is designated as positive. Moreover, in all curves, dilation and contraction are designated as negative and positive, respectively. Mention that volumetric strain is deduced by the axial strain and radial strain, expressed as Eq. (2):

$$\varepsilon_v = \varepsilon_1 - 2\varepsilon_3 \quad (2)$$

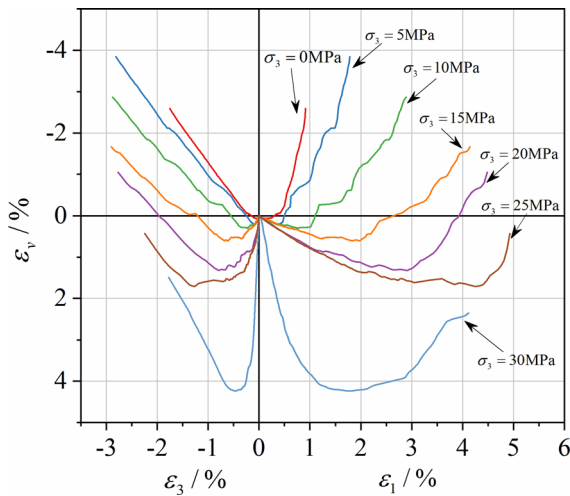


**Fig. 5** Volumetric strain versus strain curves for RCC samples under confining pressures

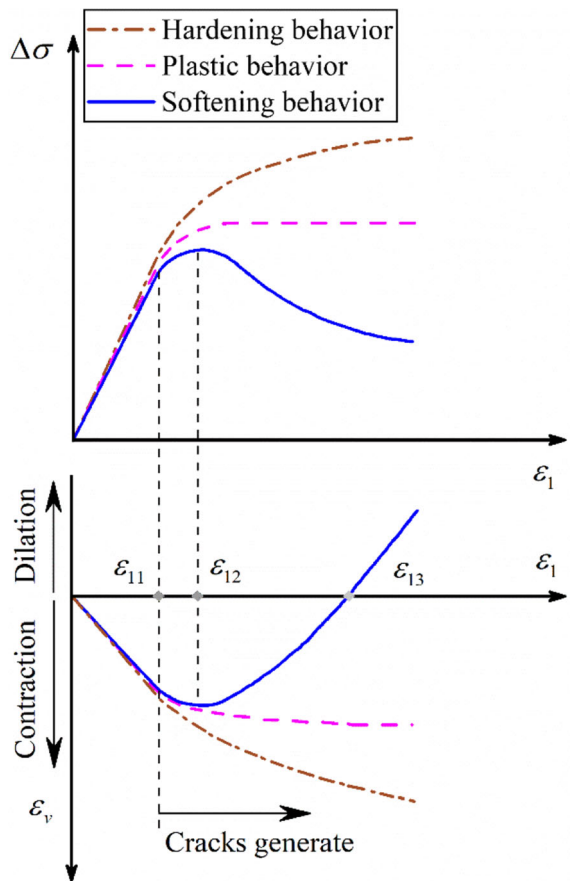


**Fig. 6** The volumetric history and compressive stress–strain curves due to three typical material behaviors

### 7 Confinement effect for RCC

The experimental responses of RCC under various confining pressures are plotted in Fig. 4 and Fig. 5. The axial deviatoric stress–strain curves and the volumetric strain history are plotted by different level of confining pressures, respectively. It’s obvious that the additional axial stress ( $\Delta\sigma = \sigma_1 - \sigma_3$ ) of RCC specimens increases significantly with increasing confining pressure at given strain. Furthermore, RCC sample shows ductile and plastic behavior in the presence of higher confinement.

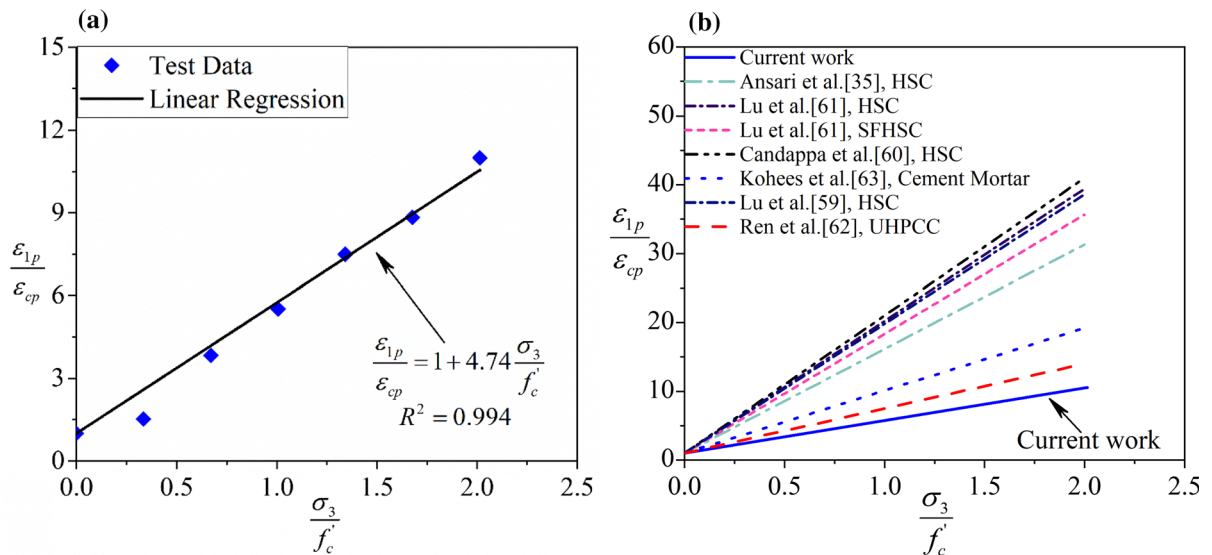
Figure 6 shows three typical relationships between the volumetric history and the compressive stress–strain curves on account of three types of material behavior: softening, plastic and hardening behavior. As the figure shows, the additional axial stress versus axial strain curve deviates from linearity at the end of elastic behavior (point  $\epsilon_{11}$ ). Correspondingly, the samples are contracted at a slower rate due to the initiation of micro-cracks [53]. For softening behavior, the volumetric strain becomes expansive beyond the point  $\epsilon_{12}$  owing to the generation of multiple cracks. Also, the volumetric history curve turns to be expansive beyond the point  $\epsilon_{12}$ . At point  $\epsilon_3$ , the specimen turns from contraction to expansion.

During the increase of axial load, RCC specimens contract axially. Meanwhile, due to Poisson’s law, lateral dilation can be observed accompanied by axial contraction. The above process is accompanied by the generation and propagation of cracks, while the confining pressure places a restriction on the development of these cracks. According to Fig. 4 ~ Fig. 6, softening behavior can be observed for RCC specimens under all confining pressures (0–30 MPa). Well-defined peak loads and smoothly descending post-peak curves can be observed. Also, the peak point moves towards coordinate origin (higher axial strain) with increasing confining pressures. As the cracks develop, the volumetric strain follows the tendency from contraction to dilation. However, when subjected to relatively higher confining pressures (15–30 MPa), the RCC specimens show more plastic behavior. The slope of post-peak curves decreases with the enhancement of confinement, which leads to horizontal plateaus. The reduction in crack developments induced by increasing confining pressures contributes to this phenomenon.



**Table 2** Triaxial compression results of RCC

$\sigma_3$ (MPa)	$\sigma_3/f'_c$	Peak additional axial stress $\Delta\sigma_p$ (MPa)	Peak axial strain $\varepsilon_{1p}/\%$	Peak lateral strain $\varepsilon_{3p}/\%$
0	0.00	14.9	0.411	-0.237
5	0.34	26.1	0.625	-0.490
10	0.67	37.3	1.578	-0.760
15	1.01	41.9	2.270	-1.279
20	1.34	50.3	3.078	-2.228
25	1.68	54.1	3.630	-2.849
30	2.01	60.1	4.516	-3.478

**Fig. 7** a  $\frac{\varepsilon_{1p}}{\varepsilon_{cp}} - \frac{\sigma_3}{f'_c}$  relationship for RCC under triaxial compression; b  $\frac{\varepsilon_{1p}}{\varepsilon_{cp}} - \frac{\sigma_3}{f'_c}$  relationships in other studies

### 7.1 Axial strain at peak axial stress

Under a range of confining pressures from 0 to 30 MPa in triaxial compression, test results are shown in Table 2, including the peak additional axial stress ( $\Delta\sigma_p$ ), the peak axial ( $\varepsilon_{1p}$ ) and lateral strain ( $\varepsilon_{3p}$ ). These results are from the average of specimens.

It's evident that the peak axial strain ( $\varepsilon_{1p}$ ) and peak lateral strain ( $\varepsilon_{3p}$ ) increases pronouncedly with the increase of the confining pressures. Figure 7 shows the relationship between normalized peak axial strain ratio ( $\varepsilon_{1p}/\varepsilon_{cp}$ ) and confinement ratio ( $\sigma_3/f'_c$ ), in which  $\varepsilon_{cp}$  denotes the peak axial strain of RCC under uniaxial compression. A linear relationship between  $\varepsilon_{1p}/\varepsilon_{cp}$  and  $\sigma_3/f'_c$  with a correlation coefficient of 0.994 ( $R^2 = 0.994$ ) can be expressed as follows:

$$\frac{\varepsilon_{1p}}{\varepsilon_{cp}} = 1 + 4.74 \frac{\sigma_3}{f'_c} \quad (3)$$

The slope of the fitted line for RCC is 4.74. In other words, the peak strain of RCC under high confining pressure ( $\sigma_3/f'_c = 1$ ) can increase by approximately fivefold than that under uniaxial compression. Similarly, the linear trend above was also found in HSC [34, 54–56], UHPCC [57], cement mortar [58] with a range of slope from 6.24 to 20. It indicates that the effect of confinement on the enhancement of peak axial strain was not pronounced for RCC, compared with HSC.

This difference between RCC and HSC mainly attributes to the relatively poor mechanical properties (tensile strength and shear strength) of the mortar matrix. There are more capillary pores in the mortar



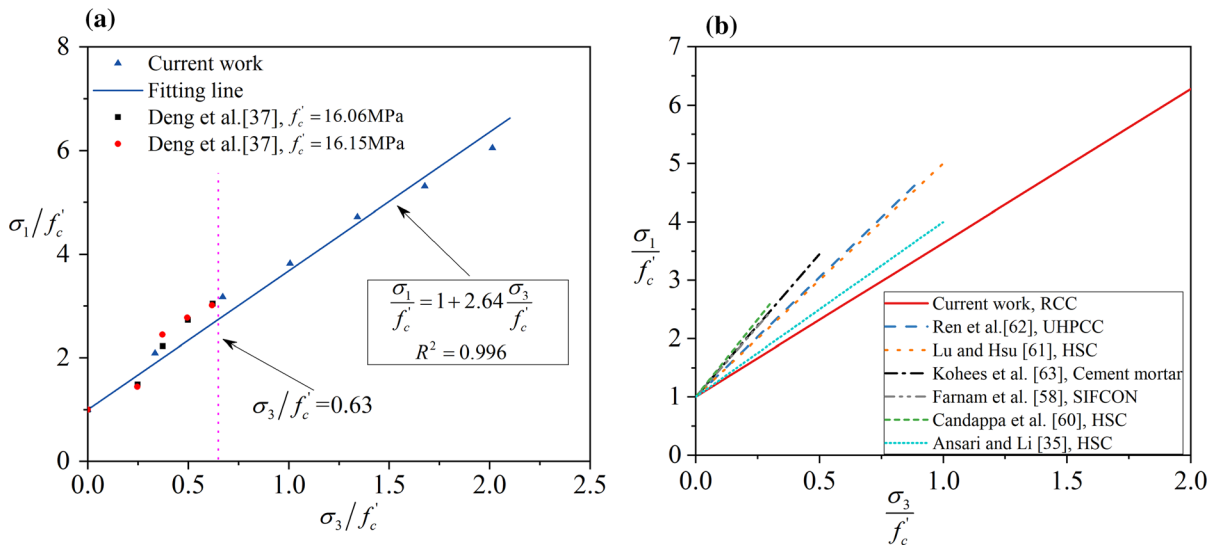


**Fig. 8** a Regression of Mohr–Coulomb failure criterion for RCC; b Regression of Mohr–Coulomb failure criterion in other studies

**Table 3** Empirical coefficients for Mohr–Coulomb failure criterion

	Specimens	$f'_c$ /MPa	Maximum of $\sigma_3/f'_c$	$k$
Farnam et al. [53]	HSC	76	0.28	4.46
	HPFRC	87	0.25	4.82
	SIFCON5	146	0.15	4.82
	SINCON10	171	0.13	4.37
Ansari and Li [34]	HSC	47	0.90	3.00
		71	0.90	2.60
		107	0.80	2.60
Lu and Hsu [55]	HSC	67	0.80	4.00
	SFHSC	69	1.00	3.95
Candappa et al. [54]	HSC	61	0.20	5.30
		73	0.20	5.30
		103	0.10	5.30
Current work	RCC	14.9	2.01	2.46

matrix of RCC, due to the low hydration degree of fly ash at an early age. Moreover, the process of drilling and grinding may bring more micro defects, which further reduce the capacity of the mortar matrix. Due to Poisson’s law, the specimens dilate laterally with axial contraction. Thus, the RCC specimens fail more easily because of lower tensile and shear properties, and the effect of confining pressures is relatively insignificant.

### 8 Failure criterion calibration

In this section, the obtained experimental results of RCC are employed to calibrate some existing failure criteria.

### 9 Mohr–Coulomb failure criterion

The Mohr–Coulomb failure criterion model [59] is a kind of pressure-dependent failure criteria and assumes only two different failure modes: the sliding failure and the separation failure. Because of its



simplicity and good accuracy, this failure criterion is still utilized extensively. The Mohr–Coulomb failure criterion can be expressed as the following equation:

$$\frac{\sigma_1}{f'_c} = 1 + k \frac{\sigma_3}{f'_c} \tag{4}$$

where  $\sigma_1$  denotes the axial stress;  $\sigma_3$  denotes the confining pressure;  $k = \frac{1+\sin \varphi}{1-\sin \varphi}$  and  $\varphi$  denotes the internal-friction angle;  $f'_c$  represents the uniaxial compressive strength.

For the present work, the linear fit to experimental data can be mathematically described by the relationship as follows

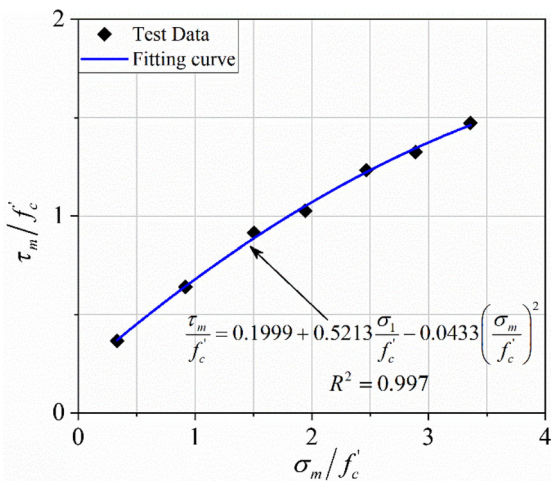


**Fig. 9** Regression of compressive meridian of RCC in this study

**Table 4** Empirical coefficients for William-Warnke failure criterion

	Specimens	$f'_c$ /MPa	Maximum of $\sigma_3/f'_c$	$a_0$	$a_1$	$a_2$
Farnam et al. [53]	HSC	76	0.28	0.177	0.560	0.019
	HPFRC	87	0.25	0.036	1.154	-0.476
Ansari and Li [34]	HSC	47	0.90	0.157	0.668	-0.120
		71	0.90	0.141	0.753	-0.208
		107	0.80	0.149	0.721	-0.196
Lu and Hsu [55]	HSC	67	0.80	0.164	0.638	-0.054
	SFHSC	69	1.00	0.160	0.653	-0.055
Candappa et al. [54]	HSC	61	0.20	0.162	0.610	-0.013
		73	0.20	0.053	1.062	-0.384
		103	0.10	0.035	1.162	-0.519
Current work	RCC	14.9	2.01	0.20	0.521	-0.0433

$$\frac{\sigma_1}{f'_c} = 1 + 2.64 \frac{\sigma_3}{f'_c} \tag{5}$$

In this case, the coefficient of correlation is 0.998 ( $R^2 = 0.998$ ). The best-fit value of  $k$  for RCC is 3.65, and the internal-friction angle  $\varphi$  can be adopted as  $34.7^\circ$ . Figure 8 (a) shows the regression relationship of the Mohr–Coulomb failure criterion. Also, the available triaxial compressive test data [40] on RCC is also given in Fig. 8 (a), yet the maximum of confining pressure is limited to 10 MPa ( $\sigma_3/f'_c < 0.63$ ). As shown in Fig. 8 (a), the  $k$  value extracted from the present study is also suitable for available experimental data of RCC.

By comparison, much previous research about  $k$  value for concrete materials has been done, in which  $k$  value scattered from 2.6 to 5.3 [34, 39, 53–56, 60–62]. As shown in Fig. 8 (b) and Table 3, the  $k$  value for RCC material is lower than HSC (High Strength Concrete), UHPCC (Ultra-high Performance Cementitious Composites), SIFCON (Slurry Infiltrated Fibre Concrete). This difference indicates that the effect of confining pressure on the peak axial strength of RCC specimens is less significant than that of other concrete materials.

Nonlinear characteristics between  $\frac{\sigma_1}{f'_c}$  and  $\frac{\sigma_3}{f'_c}$  can be found in Fig. 8 (a). Apparently,  $k = 2.64$  low-estimates underestimates the peak axial stress ( $\sigma_1$ ) values once the confinement ratio is lower than 1.0. Correspondingly, for high levels of confining pressure ( $\sigma_3/f'_c > 1.5$ ),  $k = 2.64$  overpredicts the peak stresses. This nonlinear characteristic is in accordance with previous studies on other concrete material.



## 10 William-Warnke failure criterion

The William-Warnke failure criterion [63] is a known five-parameter model. It is widely used and has been adopted in finite element analysis of concrete material. The William-Warnke failure criterion has curved compressive meridians expressed by the following form:

$$\frac{\tau_m}{f'_c} = a_0 + a_1 \left( \frac{\sigma_m}{f'_c} \right) + a_2 \left( \frac{\sigma_m}{f'_c} \right)^2 \quad (6)$$

where  $\sigma_m$  and  $\tau_m$  denote mean normal stress and mean shear stress respectively,  $\sigma_m = I_1/3 = (\sigma_1 + \sigma_2 + \sigma_3)/3$  and  $\tau_m = \left[ (\sigma_1 - \sigma_2)^2 + (\sigma_2 - \sigma_3)^2 + (\sigma_3 - \sigma_1)^2 \right]^{1/2} / \sqrt{15}$ , and  $\sigma_1, \sigma_2, \sigma_3$  represent stresses in three principle directions,  $a_0, a_1, a_2$  are coefficients of the William-Warnke failure criterion. In these coefficients,  $a_2$  shows the curve convexity of the experimental results.

Figure 9 illustrates the compressive meridian of RCC. In this study, the compressive meridian of RCC can be expressed as Eq. (7):

$$\frac{\tau_m}{f'_c} = 0.1999 + 0.5213 \frac{\sigma_m}{f'_c} - 0.0433 \left( \frac{\sigma_m}{f'_c} \right)^2 \quad (7)$$

According to the curve fitting results of RCC, the  $a_2$  coefficient, which shows the curve convexity, is nearly zero. Thus, the mean shear stress ( $\tau_m$ ) is approximately a linear function of the mean normal stress ( $\sigma_m$ ). The model coefficients of other concrete materials in literature are given in Table 4. It's noticeable that there is a similar nonlinear and parabolic relationship between  $\tau_m$  and  $\sigma_m$  for HSC, HPFRC, and SFHSC.

## 11 Conclusions

In this paper, the stress–strain responses of RCC subjected to triaxial compression have been investigated by means of the designed experimental program. Based on the experimental results and related studies, conclusions can be drawn as follows:

(1)The confinement effect of RCC is less remarkable than that of conventional concrete. The increasing confining pressure increases the peak axial stress and peak axial strain of RCC. While the effect of confinement on peak axial stress of RCC is observed

to be not as pronounced as that on conventional concrete and HRC.

(2)The peak axial strain was shown to have a linear relationship with confining pressures. When subjected to high confining pressure ( $\sigma_3/f'_c = 1$ ), there is an approximately fivefold increase in failure strain.

(3)Parameters of the Mohr–Coulomb and William-Warnke failure criterion have been calibrated. The regression curve of Mohr–Coulomb failure criterion indicates a nonlinear characteristic between peak axial stress and confining pressures. Accordingly, the  $k$  value ( $k=2.64$ ) was found to overpredict the peak stresses at higher confinements ( $\sigma_3/f'_c > 1.5$ ). Compared to other concrete material, the  $k$  value for RCC is relatively lower.

Looking forward, further investigation on triaxial behavior of RCC with different mixture compositions is crucial. The effect of fly ash content, porosity, and aggregate volume on triaxial behavior of RCC still need further study. Moreover, the relationship between interlayer quality of RCC and triaxial behavior remains largely unclear.

**Acknowledgements** This study was funded by National Natural Science Foundation of China (51979188; 51779168), by Foundation for Innovative Research Groups of the National Natural Science Foundation of China (51621092).

### Compliance with ethical standards

**Conflict of interest** The authors declare that they have no conflict of interest.

## References

1. Abdel-Halim MAH, Al-Omari MA, Iskender MM (1999) Rehabilitation of the spillway of Sama El-Serhan dam in Jordan, using roller compacted concrete. *Eng Struct* 21(6):497–506. [https://doi.org/10.1016/S0141-0296\(97\)00224-1](https://doi.org/10.1016/S0141-0296(97)00224-1)
2. Liu G, Lu W, Lou Y, Pan W, Wang Z (2018) Interlayer shear strength of Roller compacted concrete (RCC) with various interlayer treatments. *Constr Build Mater* 166:647–656. <https://doi.org/10.1016/j.conbuildmat.2018.01.110>
3. Wei B, Gu M, Li H, Xiong W, Xu Z (2018) Modeling method for predicting seepage of RCC dams considering time-varying and lag effect. *STRUCT CONTROL HLTH* 25(2):e2081. <https://doi.org/10.1002/stc.2081>
4. Yang L, Shi JJ (2009) Experimental study on the impact of rainfall on RCC construction. *J CONSTR ENG M*



- 136(5):477–483. [https://doi.org/10.1061/\(asce\)co.1943-7862.0000156](https://doi.org/10.1061/(asce)co.1943-7862.0000156)
5. Engineers UACO (2000) Roller-Compacted Concrete. EM 1110-2-2006 Department of the Army, Washington, DC
  6. Gao P, Wu S, Lin P, Wu Z, Tang M (2006) The characteristics of air void and frost resistance of RCC with fly ash and expansive agent. *Constr Build Mater* 20(8):586–590. <https://doi.org/10.1016/j.conbuildmat.2005.01.039>
  7. Hansen KD, Reinhardt WG (1991) Roller-compacted concrete dams. McGraw-Hill, New York
  8. Yerramala A, Babu KG (2011) Transport properties of high volume fly ash roller compacted concrete. *Cem Concr Compos* 33(10):1057–1062. <https://doi.org/10.1016/j.cemconcomp.2011.07.010>
  9. Warren T, Fossum A, Frew D (2004) Experimental investigation of size effect in concrete fracture under multiaxial compression into low-strength (23MPa) concrete: target characterization and simulations. *Int J Impact Eng* 30:477–503. <https://doi.org/10.1007/s10704-006-6728-7>
  10. Zhang S, Wang X, Wang C, Song R, Huo H (2017) Compressive behavior and constitutive model for roller compacted concrete under impact loading: considering vertical stratification. *Constr Build Mater* 151:428–440. <https://doi.org/10.1016/j.conbuildmat.2017.06.113>
  11. Liu D, Li Z, Liu J (2015) Experimental study on real-time control of roller compacted concrete dam compaction quality using unit compaction energy indices. *Constr Build Mater* 96:567–575. <https://doi.org/10.1016/j.conbuildmat.2015.08.048>
  12. Liu D, Liu J, Xuan P, Li Z (2016) RCC compacting mechanism and impact of VC value on compaction quality. *Water Resour Power* 34(5):128–131
  13. Ou Z, Wang H, Shan K (1989) Research on VC value of roller compacted concrete. *Hydropower and New Energy* 1:27–30
  14. Tian Y (2007) Analysis and discussions on the VC values of roller compaction concrete. *Water Power* 33(2):46–48
  15. Schrader EK (1985) Watertightness and Seepage Control in Roller Compacted Concrete Dams. *Roller Compacted Concrete*. ASCE, USA, pp 11–30
  16. Li X, Fang K (2008) Permeability of hydraulic roller compacted concrete under soft water. *J Yangtze River Sci Res Inst* 4(326):334
  17. Ruan Y, Fang K, Zeng L, Wu D (2001) Study on permeability and leakage dissolution of RCC in different hydraulic slope. *J Wuhan Univ Hydraul Electr Eng* 3(876):886
  18. Lou Y (2015) Study on the effects of layer processing on the layer adhesion properties of RCC. Zhejiang University, Master
  19. McLean FG, Pierce JS (1988) Comparison of joint shear strengths for conventional and roller compacted concrete. *Roller Compacted Concrete II*. ASCE, USA, pp 151–169
  20. Husein Malkawi AI, Mutasher SA, Qiu TJ (2003) Thermal-structural modeling and temperature control of roller compacted concrete gravity dam. *J Perform Constr Facil* 17(4):177–187. [https://doi.org/10.1061/\(asce\)0887-3828\(2003\)17:4\(177\)](https://doi.org/10.1061/(asce)0887-3828(2003)17:4(177))
  21. Jaafar M, Bayagoob K, Noorzaei J, Thanoon WA (2007) Development of finite element computer code for thermal analysis of roller compacted concrete dams. *Adv Eng Software* 38(11–12):886–895. <https://doi.org/10.1016/j.advengsoft.2006.08.040>
  22. Tatro SB, Schrader EK 1985 Thermal considerations for roller-compacted concrete. In: *Journal Proceedings* 2 119–128 Doi: <https://doi.org/10.14359/10319>
  23. Zhang G, Liu G, Liu Z (1996) Technology and simulation of temperature field for the integral roller compacted concrete arch dam. *Journal of Tsinghua University (Science and Technology)* 36:1–7. <https://doi.org/10.16511/j.cnki.qhdxxb.1996.01.001>
  24. Cao C, Sun W, Qin H (2000) The analysis on strength and fly ash effect of roller-compacted concrete with high volume fly ash. *Cem Concr Res* 30(1):71–75. [https://doi.org/10.1016/s0008-8846\(99\)00203-3](https://doi.org/10.1016/s0008-8846(99)00203-3)
  25. Lam MN-T, Le D-H, Jaritngam S (2018) Compressive strength and durability properties of roller-compacted concrete pavement containing electric arc furnace slag aggregate and fly ash. *Constr Build Mater* 191:912–922. <https://doi.org/10.1016/j.conbuildmat.2018.10.080>
  26. Wang L, Zhang G, Wang P, Yu S (2018) Effects of fly ash and crystalline additive on mechanical properties of two-graded roller compacted concrete in a high RCC arch dam. *Constr Build Mater* 182:682–690. <https://doi.org/10.1016/j.conbuildmat.2018.06.101>
  27. Fang K, Ruan Y, Zeng L (1999) Late-age properties of RCC with low cement content and high fly ash content. *J Hydro Electr Eng* 4:21–28
  28. Mardani-Aghabaglou A, Ramyar K (2013) Mechanical properties of high-volume fly ash roller compacted concrete designed by maximum density method. *Constr Build Mater* 38:356–364. <https://doi.org/10.1016/j.conbuildmat.2012.07.109>
  29. Ruan Y, FANG K, Zeng L, (2003) The Research on Pore Structure of RCC made with High-volume Fly-ash. *Fly Ash Compr Util* 000(2):23–26
  30. Wang C, Chen W, Hao H, Zhang S, Song R, Wang X (2018) Experimental investigations of dynamic compressive properties of roller compacted concrete (RCC). *Constr Build Mater* 168:671–682. <https://doi.org/10.1016/j.conbuildmat.2018.02.112>
  31. Zhang S, Song R, Wang C, Shang C, Wei P (2018) Modification of a dynamic constitutive model-HJC model for roller-compacted concrete and numerical verification. *J Vib Shock* 38:25–31. <https://doi.org/10.13465/j.cnki.jvs.2019.12.004>
  32. Zhang S, Song R, Wang C, Wei P (2019) Dynamic mechanical property analysis of roller-compacted concrete and damage constitutive model establishment. *J Cent South Univ (Sci Technol)* 50(01):130–138. <https://doi.org/10.11817/j.issn.1672-7207.2019.01.017>
  33. Chhorn C, Hong SJ, Lee SW (2018) Relationship between compressive and tensile strengths of roller-compacted concrete. *J Traffic Transp Eng (Engl Ed)* 5(3):215–223. <https://doi.org/10.1016/j.jtte.2017.09.002>
  34. Ansari F, Li Q (1998) High-strength concrete subjected to triaxial compression. *ACI Mater J* 95(6):747–755. <https://doi.org/10.14359/420>
  35. Li Q, Ansari F (2000) High-strength concrete in triaxial compression by different sizes of specimens. *ACI Mater J* 97(6):684–689. <https://doi.org/10.14359/9982>



36. Schmidt MJ, Cazacu O, Green ML (2009) Experimental and theoretical investigation of the high-pressure behavior of concrete. *Int J Numer Anal Methods Geomech* 33(1):1–23. <https://doi.org/10.1002/nag.700>
37. Sfer D, Carol I, Gettu R, Etse G (2002) Study of the behavior of concrete under triaxial compression. *J Eng Mech* 128(2):156–163. [https://doi.org/10.1061/\(asce\)0733-9399\(2002\)128:2\(156\)](https://doi.org/10.1061/(asce)0733-9399(2002)128:2(156))
38. Vu XH, Daudeville L, Malecot Y (2011) Effect of coarse aggregate size and cement paste volume on concrete behavior under high triaxial compression loading. *Constr Build Mater* 25(10):3941–3949. <https://doi.org/10.1016/j.conbuildmat.2011.04.026>
39. Xie J, Elwi A, MacGregor J (1995) Mechanical properties of three high-strength concretes containing silica fume. *ACI MATER J* 92(2):135–145. <https://doi.org/10.14359/9764>
40. Deng RG (2002) Mechanical properties of roller compacted concrete. *J Southwest Jiaotong Univ* 25(3):147–152
41. sAFM Regulation, SAotPsRo China (2017) Moderate-heat portland cement, low-heat portland cement, vol GB 200–2003. Standards Press of China, Beijing
42. Administration NE (2014) Technical code for chemical admixtures for hydraulic concrete. China Electric Power Press, Beijing
43. Commission NDaR (2007) Technical specification of fly ash for use in hydraulic concrete. China Electric Power Press, Beijing
44. Kong Y (2014) Methods for confirming parameters of dynamic damage constitutive model for RCC under high strain rates. Tianjin University, China
45. Zhang S, Song R, Wang C, Wang X (2018) experimental investigation of the compressive behavior of RCC under high strain rates: considering the rolling technique and layered structure. *J Mater Civ Eng* 30(4):04018057. [https://doi.org/10.1061/\(asce\)jmt.1943-5533.0002223](https://doi.org/10.1061/(asce)jmt.1943-5533.0002223)
46. Liu Z (1982) Sealing and oil proofing of rock specimens in triaxial test. *Quarterly of CIMR* 2(3):7
47. Wang B, Yang T, Zhang L (2008) Rock mechanics experiment guide. University of Science and Technology Beijing, School of Civil and Environmental Engineering
48. Xu X (2016) Experimental Study on Mechanical Properties of Shaft Lining High Strength Concrete under Hydraulic Pressure China. University of Mining and Technology, Beijing
49. Guo Z (1997) Strength and deformation of concrete-experimental principle and constitutive law. Tsinghua University Press House, Beijing, China
50. Li B, Xiong H, Jiang J (2018) End-friction effect on concrete cubes with passive confinement. *J Mater Civ Eng* 30(8):04018194. [https://doi.org/10.1061/\(asce\)jmt.1943-5533.0002336](https://doi.org/10.1061/(asce)jmt.1943-5533.0002336)
51. Mier JGMV, Shah SP, Arnaud M, Balaýssac JP, Bascoul A, Choi S, Dasenbrock D, Ferrara G, French C, Gobbi ME (1997) Strain-softening of concrete in uniaxial compression. *Mater Struct* 30(4):195–209. <https://doi.org/10.1007/bf02486177>
52. Xiao P, Li B, Jiang J (2015) Effect of friction-reducing padson concrete under compression. *J Mater Sci Eng* 33(1):127–132. <https://doi.org/10.14136/j.cnki.issn1673-2812.2015.01.028>
53. Farnam Y, Moosavi M, Shekarchi M, Babanajad S, Bagherzadeh A (2010) Behaviour of slurry infiltrated fibre concrete (SIFCON) under triaxial compression. *Cem Concr Res* 40(11):1571–1581. <https://doi.org/10.1016/j.cemconres.2010.06.009>
54. Candappa D, Sanjayan J, Setunge S (2001) Complete tri-axial stress-strain curves of high-strength concrete. *J Mater Civ Eng* 13(3):209–215. [https://doi.org/10.1061/\(asce\)0899-1561\(2001\)13:3\(209\)](https://doi.org/10.1061/(asce)0899-1561(2001)13:3(209))
55. Lu X, Hsu C-TT (2006) Behavior of high strength concrete with and without steel fiber reinforcement in triaxial compression. *Cem Concr Res* 36(9):1679–1685. <https://doi.org/10.1016/j.cemconres.2006.05.021>
56. Lu X, Hsu C-TT (2007) Stress-strain relations of high-strength concrete under triaxial compression. *J Mater Civ Eng* 19(3):261–268. [https://doi.org/10.1061/\(asce\)0899-1561\(2007\)19:3\(261\)](https://doi.org/10.1061/(asce)0899-1561(2007)19:3(261))
57. Ren G, Wu H, Fang Q, Liu J, Gong Z (2016) Triaxial compressive behavior of UHPCC and applications in the projectile impact analyses. *Constr Build Mater* 113:1–14. <https://doi.org/10.1016/j.conbuildmat.2016.02.227>
58. Kohees M, Sanjayan J, Rajeev P (2019) Stress-strain relationship of cement mortar under triaxial compression. *Constr Build Mater* 220:456–463. <https://doi.org/10.1016/j.conbuildmat.2019.05.146>
59. Chen WF, Han DJ (2007) Plasticity for structural engineers. J. Ross Publishing Inc., New York
60. Chern J-C, Yang H-J, Chen H-W (1993) Behavior of steel fiber reinforced concrete in multiaxial loading. *ACI Mater J* 89(1):32–40. <https://doi.org/10.14359/1242>
61. Imran I, Pantazopoulou S (1996) Experimental study of plain concrete under triaxial stress. *ACI Mater J* 93(6):589–601. <https://doi.org/10.14359/9865>
62. Lan S, Guo Z (1997) Experimental investigation of multi-axial compressive strength of concrete under different stress paths. *ACI Mater J* 94(5):427–434. <https://doi.org/10.14359/327>
63. Chen WF (2007) Plasticity in reinforced concrete. J. Ross Publishing Inc., New York

**Publisher's Note** Springer Nature remains neutral with regard to jurisdictional claims in published maps and institutional affiliations.

